JASA ARTICLE

Analysis of supersonic jet turbulence, fine-scale noise, and shock-associated noise from characteristic, bi-conic, faceted, and fluidic injection nozzles[a)]

Trushant K. Patel[b)] and Steven A. E. Miller
Department of Mechanical and Aerospace Engineering, University of Florida, P.O. Box 116250, Gainesville, Florida 32611, USA

ABSTRACT:
Fine-scale mixing noise (FSMN) and broadband shock-associated noise (BBSAN) are the dominant components of supersonic jet noise in the sideline and upstream directions. We use the previously developed statistical FSMN and BBSAN models to compare the noise radiated from three different nozzles, i.e., a method of characteristics nozzle, a bi-conic nozzle, and a faceted nozzle at different operating conditions. A numerical sensitivity analysis is performed using the models by perturbing various model parameters and conditions such as nozzle pressure ratio (NPR), total temperature ratio, area ratio, and boundary layer thickness. We observed that FSMN is most sensitive to NPR and BBSAN is most sensitive to area ratio. We also examine the changes in source statistics and corresponding correlations of the radiated noise using the fluidic injection noise reduction technique. Noise reduction predictions relative to the baseline cases are compared at different operating conditions and similar reduction as the experimental measurements were obtained at over-expanded conditions. Finally, we analyze the noise source locations for both components of jet noise in the sideline direction. The trends predicted in this study increase understanding of the changes in source statistics and radiated noise for different nozzles over a range of operating conditions.
 https://doi.org/10.1121/10.0005626
(Received 11 March 2021; revised 17 June 2021; accepted 25 June 2021; published online 21 July 2021)
[Editor: Philip J. Morris] Pages: 490–505

I. INTRODUCTION

Jet noise is detrimental to the health and hearing of military personnel working in close proximity to flight-vehicles on an aircraft carrier. The intensity of jet noise on an aircraft carrier deck ranges from 120 to 150 dB at peak frequencies.[1] Approximately 800×10^6 dollars were spent by the US Department of Veterans Affairs for hearing loss disability benefits in 2005. That number has risen to over a billion dollars in the last decade.[1] Therefore, it is vital to reduce the jet noise for the health of military personnel employed on aircraft carriers. Furthermore, reducing jet noise is beneficial for surrounding communities near civilian and military airports. In order to minimize jet noise, understanding the source mechanism and the sensitivity of the jet noise on different parameters is very important. In this paper, we perform sensitivity analyses on two components of supersonic jet noise using previously developed closed-form statistical models.[2,3] We perturb the nozzle pressure ratio (NPR), total temperature ratio (TTR), area ratio, and the nozzle exit boundary layer profile and analyze the associated changes in the source intensity and the radiated noise. We also examine an active fluidic injection noise reduction technique using the developed statistical models.

The noise from a supersonic jet operating at an off-design condition is generally categorized into turbulent mixing noise and shock-associated noise. The turbulent mixing noise can be further categorized into fine-scale mixing noise (FSMN) and large-scale mixing noise (LSMN), while the shock-associated noise consists of two components, broadband shock-associated noise (BBSAN) and "screech" tones. An excellent review article on the different components of supersonic jet noise is written by Tam.[4] The generation mechanism and directivity of each component of supersonic jet noise are different. FSMN and LSMN radiate from the fine-scale and large-scale turbulent structures, respectively. LSMN is dominant in the downstream direction and FSMN has a relatively uniform directivity. Also, LSMN spectrum contains a narrow peak and FSMN spectrum has a broad peak. BBSAN is generated because of the interaction of coherent large-scale turbulent structures with the shock-cell structure and is dominant in the sideline and upstream directions. Screech tones consist of multiple discrete frequencies and are generated due to a feedback mechanism between upstream traveling waves coupled with the downstream traveling instabilities. In this paper, we focus on FSMN and BBSAN, as they are the dominant components of jet noise in the sideline and upstream directions.

Various prediction models for FSMN and BBSAN have been proposed by different investigators. Harper-Bourne and Fisher[5] were the first to investigate and develop an empirical model of the two-point cross-correlation of pressure at different shock locations to predict BBSAN. Overcoming some of the limitations of the Harper-Bourne

[a)]This paper is part of a special issue on Supersonic Jet Noise.
[b)]Electronic mail: ptrushant@gmail.com

https://doi.org/10.1121/10.0005626

and Fisher[5] model, a theory based on the physics of BBSAN was proposed by Tam and Tanna.[6] Later, Tam[7] developed a stochastic model that built upon the theory of Tam and Tanna.[6] Using the work of Tam[7] as a basis, Morris and Miller[8] developed a prediction model for BBSAN. They used Reynolds-averaged Navier–Stokes (RANS) computational fluid dynamics (CFD) simulations as an argument for their model. Suzuki[9] created a model to predict BBSAN using wave-packet theory and large-eddy simulation (LES) data. For FSMN prediction, a statistical model was developed by Tam and Auriault[10] by considering the source and propagating terms separately. Patel and Miller[2,3] identified the statistical source terms for FSMN and BBSAN from the Navier–Stokes equations using the decomposition approach of Miller.[11] They developed statistical models by convolving the identified source terms with the vector Green's function. Using the identified source terms from the Navier-Stokes equations reduces some of the empiricism associated with the modeling of the source term. In the present work, we perform various analyses to ascertain the effect of different parameters using the developed statistical models.[2,3]

Dahl and Kharavan[12] performed a sensitivity analysis of the BBSAN model developed by Tam.[7] They replaced the fixed model parameters with probabilistic distributions and examined the effect of different input parameters on the radiated noise. They considered twelve parameters in the BBSAN model of Tam[7] and identified four parameters that maximally affected the BBSAN spectrum. These four parameters were associated with the convective velocity, lowest and second-lowest wave-number mode of the shock-cell structure, and the half-width of the similarity source. Freund[13] and Kim *et al.*[14] performed a sensitivity analysis using adjoint-based methods in conjunction with LES to reduce the noise from an ideally expanded Mach 1.3 turbulent jet. A reduction of 3.5 dB was obtained by Kim *et al.*[14] *via* controlling the parameters in the near nozzle region of the jet. In the present paper, we perform a similar sensitivity analysis of FSMN and BBSAN models. We perturb different model parameters and input conditions (e.g., NPR, TTR, area ratio, boundary layer profile, and nozzle geometry) by a small amount to ascertain the parameters that have the maximum effect on the radiated noise.

Extensive experiments were performed by Tanna,[15] Seiner and Norum,[16,17] Norum and Seiner,[18–20] and Seiner and Yu[21] to understand the dependence of BBSAN on various input parameters. Norum and Seiner,[18] and Tanna[15] observed that the BBSAN becomes important relative to the turbulent mixing noise when the NPR deviates from the design condition, TTR decreases, and when the observer is not in the downstream radiation direction. Different experiments were performed by Bridges and Wernet,[22] Viswanathan *et al.*,[23] and Kuo *et al.*[24] to understand the effect of temperature on BBSAN. A numerical study on the effect of temperature on BBSAN was performed by Miller.[25] It was observed that the BBSAN increases with an increase in TTR to a certain level and remains constant thereafter. For a given NPR, the intensity of the shock-cell structure in the exhaust of the nozzle can be controlled by altering the area ratio of the nozzle. Variable area nozzles are used in various military aircrafts such as the F-15 and F-16, and were studied by Mabe[26] and Michel.[27] The variation of fine-scale mixing noise with different jet exit velocities and temperature ratios were examined by Tam and Auriault[10] and Tam *et al.*[28]

The effect of noise from different nozzle geometries has been investigated by various researchers. Saleem *et al.*[29] compared the acoustic spectrum from a faceted nozzle with a baseline bi-conic nozzle and observed a very similar acoustic spectrum and overall sound pressure level (OASPL). For subsonic jet noise, Zaman[30] compared the noise from two nozzles having different exit boundary layer profiles. He found the nozzle with a laminar boundary layer at the nozzle exit to be noisier than the nozzle with a turbulent boundary layer. Bogey and Bailly[31] and Bogey *et al.*[32] studied the boundary layer profile at the exit of the nozzle numerically using LES. They numerically tripped the boundary layer inside the nozzle and observed that the jet noise is reduced. Brès *et al.*[33] related the reduction of noise from the turbulent boundary layer variation to the difference in the growth rate of the Kelvin-Helmholtz modes in the near nozzle region observed. As BBSAN is generated due to the interaction of the coherent large-scale turbulent structures with the shock-cell structure, any effect of the boundary layer on the large-scale turbulent structures may affect the BBSAN. The source location of fine-scale noise also changes with a change in the boundary layer profile at the nozzle exit.[34]

Many researchers have proposed different techniques to reduce jet noise such as porous nozzle plugs,[35] mixer ejectors,[36] chevrons,[37] beveled nozzles,[38] corrugated nozzles,[39,40] fluidic injection,[41] plasma actuation,[42] etc. In this paper, we will use the developed statistical models for FSMN and BBSAN to examine the fluidic injection noise reduction technique. The fluidic injectors break down the shock-cells into smaller and weaker structures, and thereby reduce BBSAN. The fluidic injection also affects the boundary layer near the nozzle, thereby altering the growth of the instability waves and reduces the large-scale mixing noise too. Morris *et al.*[41] designed the location and angles of fluidic inserts using previous studies on supersonic transverse jets.[43,44] They also performed various experiments and observed a reduction of 4 dB in turbulent mixing noise and 2 dB in shock-associated noise. Powers *et al.*[45] compared the aerodynamics of the corrugated nozzles with the fluidic injections using laser Doppler velocimetry measurements and RANS CFD simulations. Moderate-scale experiments of the fluidic inserts were performed by McLaughlin *et al.*[46] in the General Electric Aviation Cell 41 Laboratory and similar noise reduction results as the small-scale experiments were observed. Various numerical investigations to better understand the noise reduction mechanism have been carried out by Prasad and Morris,[47] Morris *et al.*,[48] Coderoni *et al.*,[49] and Cuppoletti *et al.*[50] using RANS and LES solutions.

The rest of the paper is organized as follows. The developed statistical models for FSMN and BBSAN are summarized in Sec. II. The sensitivity analyses of the developed

FSMN and BBSAN models are performed in Sec. III. We perturb various model parameters of the developed FSMN and BBSAN models in Sec. III A. The effect on radiated noise from different nozzle geometries is discussed in Sec. III B. The effect of perturbation of different input conditions such as NPR, TTR, and area ratio is analyzed in Sec. III C. We also analyze the change in radiated noise due to a change in the boundary layer thickness at the nozzle exit in Sec. III D. Finally, the fluidic injection noise reduction technique is analyzed using the developed statistical models in Sec. IV.

II. STATISTICAL MODELS

The field variables in the Navier–Stokes equations are decomposed into a time-averaged base flow, aerodynamic turbulent fluctuations due to fine-scale and large-scale structures, and radiating acoustic fluctuations. All the source terms, i.e., time-averaged base flow and aerodynamic turbulent fluctuations, are brought to the right-hand side and the radiating acoustic fluctuations are brought to the left-hand side. The spectral density of pressure is obtained by convolving the dominant statistical source term of FSMN and BBSAN with the vector Green's function of pressure. The dominant statistical source terms for FSMN and BBSAN have been identified by Patel and Miller.[2,3] The identified source terms for FSMN and BBSAN are

$$\left\langle \frac{D\breve{p}^{(1)}}{Dt}, \frac{D\breve{p}^{(2)}}{Dt} \right\rangle, \quad \frac{(\gamma-1)}{2}\left\langle \frac{D\breve{p}^{(1)}}{Dt}, \frac{D\bar{\rho}^{(2)}\breve{u}_k^{(2)}\breve{u}_k^{(2)}}{Dt} \right\rangle, \quad \frac{(\gamma-1)^2}{4}\left\langle \frac{D\bar{\rho}^{(1)}\breve{u}_k^{(1)}\breve{u}_k^{(1)}}{Dt}, \frac{D\bar{\rho}^{(2)}\breve{u}_k^{(2)}\breve{u}_k^{(2)}}{Dt} \right\rangle, \tag{1}$$

and

$$\gamma^2\left\langle \frac{\partial \hat{u}_j^{(1)}\bar{p}^{(1)}}{\partial y_j}, \frac{\partial \hat{u}_m^{(2)}\bar{p}^{(2)}}{\partial y_m} \right\rangle, \tag{2}$$

respectively. Note that all three FSMN source terms in Eq. (1) have the same scaling. Also, the third term in Eq. (1) is the same source term for FSMN as identified by Tam and Auriault[10] using the gas kinetic theory. Here, ρ, p, and $\boldsymbol{u}$ represent the density, pressure, and velocity of the fluid, respectively. The ratio of specific heats is denoted by γ. The overbar $\bar{\square}$ symbol represents the time-averaged quantity, the breve $\breve{\square}$ symbol represents the aerodynamic fluctuations due to fine-scale structures, and the hat $\hat{\square}$ symbol represents the aerodynamic fluctuations due to large-scale structures. The superscripts (1) and (2) denote the location of two different source terms, one at location $\mathbf{y}$ and the other at $\mathbf{y}+\boldsymbol{\eta}$. The angular brackets $\langle\square,\square\rangle$ represent the two-point cross-correlation of the source terms at two different locations.

The spectral density of pressure for FSMN and BBSAN are

$$S_{\mathrm{FSMN}}(\mathbf{x},\omega) = \left(\frac{1}{4\ln 2}\right)^{3/2}\frac{\omega^2}{16\sqrt{\pi}c_\infty^4 r^2} \times \int_{-\infty}^{\infty}\int\int\int \frac{\bar{\rho}^2 K_s^2 l_s^3}{c_A^2 \tau_s} \times \frac{\exp\left[-\dfrac{\omega^2 l_s^2}{\bar{u}^2(4\ln 2)}\right]}{\left[1+\left(1-\dfrac{\bar{u}}{c_\infty}\cos\theta\right)^2\omega^2\tau_s^2\right]} d\mathbf{y}, \tag{3}$$

and

$$S_{\mathrm{BBSAN}}(\mathbf{x},\omega) = \frac{\gamma^2\omega^2}{16\pi\sqrt{\pi}c_\infty^4 r^2}\int_{-\infty}^{\infty}\int\int\int l_\perp^2 l\tau \times \exp\left[-\frac{\omega^2 l_\perp^2\sin^2\theta}{4c_\infty^2}\right]\frac{\partial\bar{p}}{\partial y_j}\hat{u}_j \times \frac{\exp\left[-l^2\left(\kappa-\dfrac{\omega\cos\theta}{c_\infty}\right)^2/4\right]}{\left[1+\left(1-M_c\cos\theta+\dfrac{u_c\kappa}{\omega}\right)^2\omega^2\tau_s^2\right]} \times \frac{\partial\tilde{\bar{p}}}{\partial y_m}\hat{u}_m d\kappa d\mathbf{y}, \tag{4}$$

respectively. The detailed mathematical derivation of the spectral density of pressure can be found in Miller[11] and Patel and Miller.[2,3] Here, the source locations and observer locations are represented by $\mathbf{x}$ and $\mathbf{y}$, respectively. The distance from the source location to the observer location is represented by $r = |\mathbf{y}-\mathbf{x}|$. The tilde operator $\tilde{\square}$ is used to denote the Fourier transform of the variable and the wavenumber is represented by κ. The angular frequency and ambient speed of sound are denoted using ω and c_∞, respectively. The turbulent kinetic energy (TKE), length-scale in the stream-wise direction, length-scale in the cross-stream direction, and timescale are represented by K, l, $l_\perp$, and τ, respectively. The convective velocity and Mach number are denoted using u_c and M_c, respectively.

The arguments of the models such as field-variables, turbulent kinetic energy, length-scale, and time-scale are calculated from steady RANS CFD solutions. The $K-\Omega$ shear stress transport (SST) model is used to close the RANS equations, where K is the turbulent kinetic energy and Ω is the specific dissipation rate. The local length- and time-scales are estimated using the turbulent kinetic energy and dissipation rate as $l = c_l K^{3/2}\epsilon^{-1}$ and $\tau = c_\tau K\epsilon^{-1}$, respectively, where $\epsilon = 0.09K\Omega$ is the dissipation rate. The Fully Unstructured Navier–Stokes (FUN3D)[51] CFD code developed at NASA Langley Research Center is used to calculate the solution to the RANS equations. The developed FSMN and BBSAN models have been calibrated at one

https://doi.org/10.1121/10.0005626

operating condition, and the same calibration constants are used to predict noise for different jet operating conditions and different nozzle types. Very good agreement with the experimental measurements has been previously obtained.[2,3]

The computational domain for the RANS simulations is selected such that the important physics is captured inside the domain and the effect of far-field boundary conditions is minimized. The extents of the computational domain are unchanged for different nozzle types. The computational domain is extended to *100D* in the downstream direction and *50D* in the cross-stream directions from the nozzle exit, where D is the diameter of the nozzle exit. The computational domain is restricted to one quarter of the entire domain, and symmetric plane boundary conditions are enforced on the y and z planes of symmetry to reduce the computational expense. Unstructured meshes are generated for all nozzle types. The mesh is generated such that it is extremely fine inside the nozzle, in the potential core, and the shear layer regions. The boundary layer is resolved up to $y^+ = 4.5$ for the highest speed case of the method of characteristics (MOC) nozzle. A grid independence study is performed to ensure that the generated mesh does not affect the CFD solution. The total number of cells in the computational domain ranges approximately between 4 to 5×10^6 for the MOC and bi-conic nozzles, between 6 to 7×10^6 for the faceted nozzle, and between 33 to 34×10^6 for the fluidic injection nozzle. More details on the evaluation and the validation of the FSMN and BBSAN models are presented by Patel and Miller.[2,3] In Sec. III, we will perform sensitivity analyses using Eqs. (3) and (4) to understand the dependence of FSMN and BBSAN on different parameters.

III. SENSITIVITY ANALYSIS

We perform sensitivity analyses for different parameters using the developed FSMN and BBSAN models to understand the uncertainty associated with each input parameter. We perform one-at-a-time sensitivity analyses by varying one parameter by 1% while keeping all other parameters constant. The resulting change in the sound pressure level (SPL) per unit Strouhal (St) number for FSMN and BBSAN is examined using Eqs. (3) and (4), respectively. The numerical sensitivity can be calculated by performing the derivative of the SPL with respect to the change in input, i.e., $\partial(\mathrm{SPL})/\partial I$, where I is the input parameter.

Due to the differences in the closure models of the RANS equations, different RANS models may give different values of mean quantities, TKE, and specific dissipation rate. Hence, a sensitivity analysis for model parameters can identify the parameters which are most and least sensitive. The sensitivity analyses of FSMN and BBSAN on different model parameters is performed in Sec. III A. Furthermore, the flow physics from a fluidic insert nozzle is different from a conventional nozzle. Modifications are made into the faceted nozzle geometry to develop a fluidic insert nozzle. The boundary layer at the nozzle exit is thicker when compared to MOC, bi-conic, and faceted nozzles. Hence, the effect of nozzle geometry, jet operating conditions, and boundary layer thickness on FSMN and BBSAN are quantified in Secs. III B–III D, respectively. The results of these sensitivity analyses with respect to different parameters helps us understand the uncertainties associated with the predictions of noise reduction with the fluidic insert nozzle in Sec. IV.

A. Sensitivity analysis to model parameters

An SMC000 nozzle operating at an NPR = 1.893 and TTR = 3.20, corresponding to $M_j = 1.00$ is used for the sensitivity analyses of the FSMN model. The sensitivity analyses of the SPL to the model parameters for the statistical FSMN model are shown in Fig. 1(a). And the sensitivity analyses to various BBSAN model parameters are shown in Fig. 1(b) for an SMC016 nozzle operating an NPR = 5.2 and TTR = 1.0. We use the same nozzles and operating

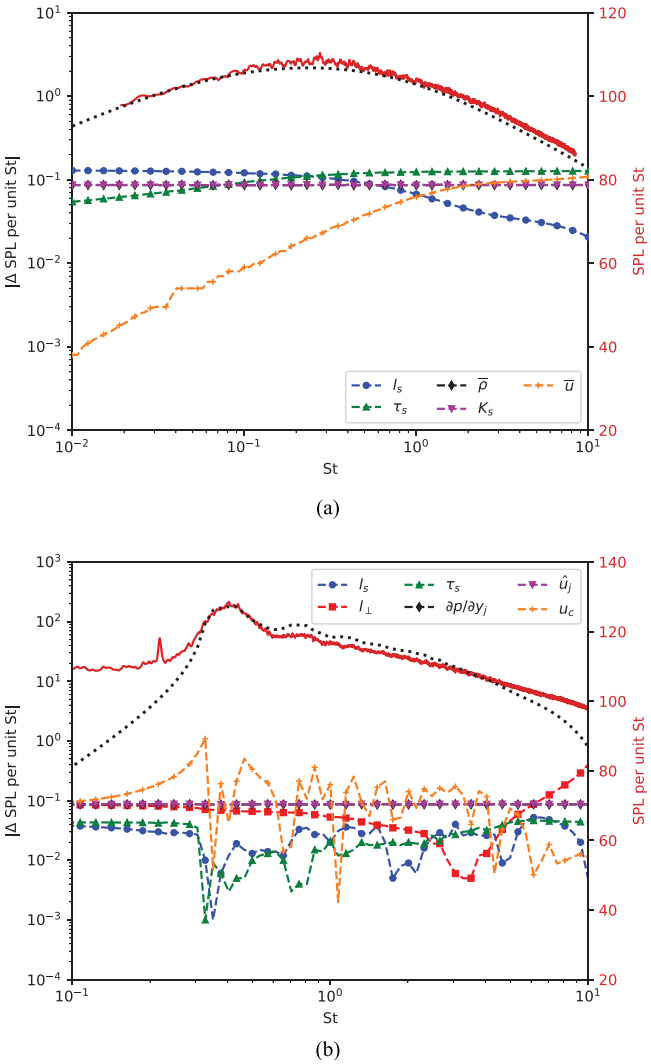

FIG. 1. (Color online) Sensitivity analyses of FSMN and BBSAN parameters. The red solid line represents the experimental spectrum and the black dotted line represents the statistical prediction. The dashed lines represent the sensitivity of model parameters. (a) Sensitivity of FSMN model parameters. (b) Sensitivity of BBSAN model parameters.

conditions for the parametric sensitivity analysis that were used to calibrate the FSMN and BBSAN models. The observer is located at a distance of *100D* in the sideline direction ($\theta = 90^\circ$). The experimental spectrum and the statistical prediction results using Eqs. (3) and (4) are superposed in Fig. 1 along with the sensitivity results. The experimental spectrum is from the Small Hot Jet Acoustic Rig (SHJAR) database[52] from NASA Glenn Research Center at Lewis Field. The detailed geometry of the SMC series nozzles is shown in Brown and Bridges.[52] A dual y axis plot is shown in Fig. 1, where the left-hand side labels represent the sensitivity of the model in terms of absolute change in the SPL per unit Strouhal number when the model parameters are perturbed. The right-hand side labels in Fig. 1 represent the SPL per unit Strouhal number of the experimental spectrum and the statistical prediction.

We observe that the sensitivity to all the model parameters is less than 0.2 dB at all St, for the sensitivity analyses of the FSMN model in Fig. 1(a). For low St, the length-scale exhibits the highest sensitivity. A change of 0.13 dB per unit St is obtained with 1% perturbation in the length-scale. However, the sensitivity to the length-scale decreases at high St and reduces to 0.018 dB per unit St at St = 10. An opposite trend is observed for the sensitivity to the mean velocity, $\bar{u}$, and timescale, τ_s. The sensitivity to mean velocity and timescale increases at different rates as St increases. At St = 10, the sensitivity to mean velocity and timescale are 0.1 and 0.12 dB per unit St, respectively. The sensitivity to TKE and mean density are 0.09 dB per unit St at all St. Hence, small perturbations in the FSMN source term cause a constant change in the SPL at all frequencies.

For the sensitivity analyses of the BBSAN model in Fig. 1(b), we observe that the sensitivity to all the parameters is less than 1 dB at all frequencies. The sensitivity to the convective velocity is the highest among all the parameters. The sensitivity to all remaining parameters is less than 0.1 dB at all frequencies. At the BBSAN peak, the sensitivity to the length-scale in the stream-wise direction and the time-scale are 0.001 dB at St = 0.4037. The sensitivity to the length-scale in the stream-wise direction and time-scale fluctuates from 0.001 to 0.045 dB per unit St at all frequencies. The sensitivity to the length-scale in the cross-stream direction decreases till St = 3.5 and increases afterward with an increase in St. Note that we are not using the frequency dependent length- and time-scales in the statistical BBSAN model. Using frequency dependent length-scales will result in lower sensitivity at high St for the length- and time-scales. The sensitivity to the gradient of mean pressure and the large-scale anisotropic velocities is constant at all frequencies. The SPL varies by 0.09 dB per unit St with a 1% change in either the gradient of mean pressure or the large-scale anisotropic velocities. Since the product of the gradient of mean pressure and the anisotropic velocities is the source term for BBSAN, any change in the parameters of the source term directly alters the noise radiated.

B. Effect of nozzle geometry

The noise radiated from three different nozzles, a method of characteristics nozzle (SMC016), a bi-conic nozzle, and a faceted nozzle are analysed in this section. The bi-conic and faceted nozzles are chosen because their shapes are more representative of a low bypass military engine nozzle. The bi-conic nozzle is designed such that the length of the diverging section matches that of the SMC016 nozzle. The coordinates of the bi-conic nozzle are tabulated in Ref. 53. In order to design a faceted nozzle, we added twelve facets to the bi-conic nozzle to convert the axisymmetric bi-conic nozzle to a faceted nozzle. The facets are designed such that the area of the exit of the faceted nozzle matches the exit area of the round nozzles. The circumradius of the faceted nozzle is 2.5992 cm.

A comparison of the Mach number contours from all three nozzles is shown in Fig. 2. All the nozzles are operating at the design condition of NPR = 3.67 and TTR = 3.0, which correspond to $M_j = M_d = 1.5$. No shocks are observed in the exhaust of the jet for the SMC016 nozzle since the reflections of the characteristics from the nozzle wall are eliminated in a MOC nozzle. However, we observe

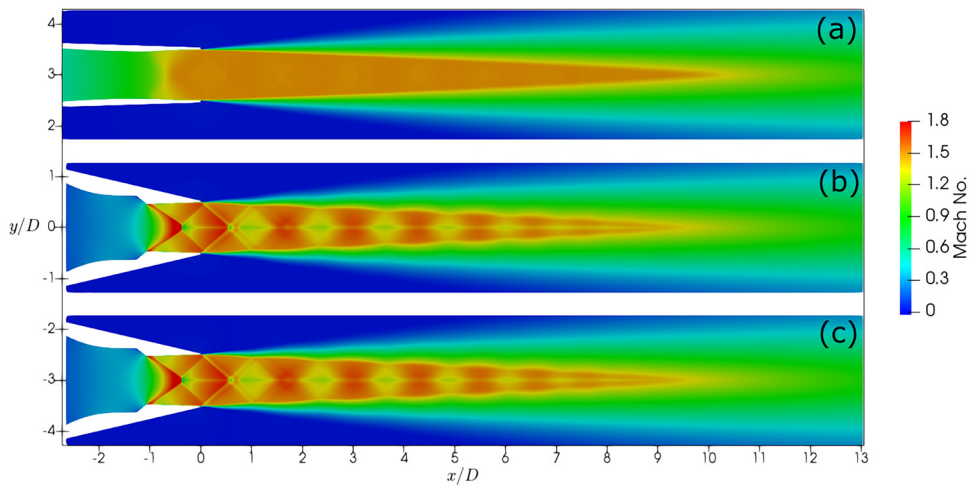

FIG. 2. (Color online) Mach number contours of (a) SMC016 nozzle, (b) bi-conic nozzle, and (c) faceted nozzle operating at design condition.

https://doi.org/10.1121/10.0005626

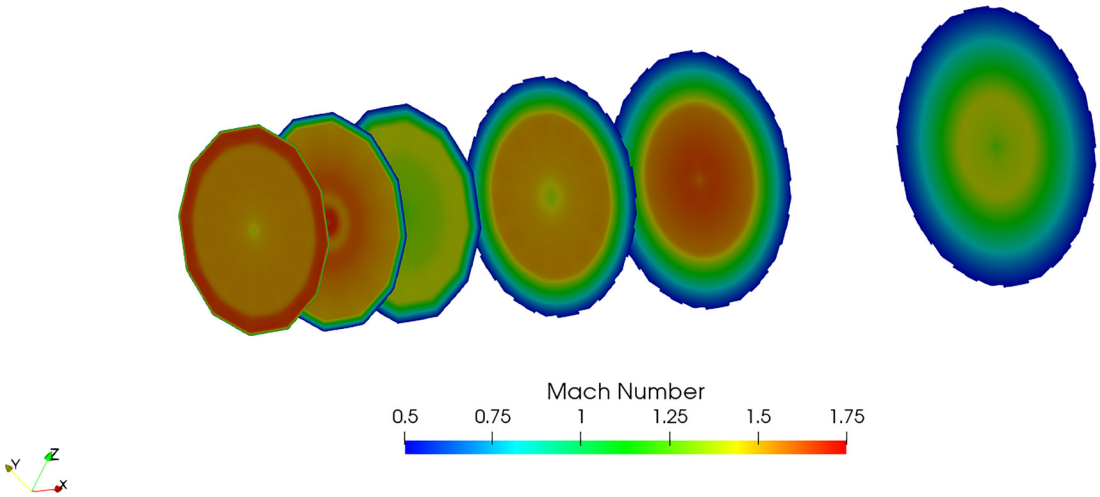

FIG. 3. (Color online) Cross-stream Mach number contours at different axial locations $x/D = 0$, 0.5, 1.0, 2.0, 3.0, and 5.0 for the faceted nozzle operating at NPR = 3.67 and TTR = 3.0.

a shock-cell structure in the jet exhaust for the bi-conic and faceted nozzle in Fig. 2 due to the planar divergent walls. The aerodynamic flow-field in the jet plume from the bi-conic and faceted nozzles at the $z/D = 0$ cross-sectional plane are very similar. The cross-stream Mach number contours at different axial locations for the faceted nozzle operating at the design condition are shown in Fig. 3. The flow-field alteration due to the facets is visible in the Mach number contours until $x/D = 2.0$ in Fig. 3. Similar qualitative cross-sectional contour plots for a 12 facet nozzle operating at a different condition were obtained by Pilon *et al.*[54]

We also compare the noise radiated from different nozzles under a range of operating conditions. The operating conditions are selected from the SHJAR database.[52] All three nozzles are operated over a range of conditions from NPR = 2.4 to 6.0 for a heated jet with TTR = 3.0. The OASPL of FSMN and BBSAN versus the fully-expanded jet Mach number for different operating conditions for an observer in the sideline direction is plotted in Fig. 4. The noise for the SMC016 nozzle is reduced at the design condition, while the noise remains almost constant for the bi-conic and faceted nozzle. This is because no shocks are present at the design condition for the SMC016 nozzle, while a shock-cell structure is present for the bi-conic and faceted nozzles. The OASPL from the bi-conic nozzle and faceted nozzle at different NPRs in the sideline direction are within 2 dB of each other. Similar results have been obtained from the experimental measurements by various researchers.[29,55] The BBSAN intensity is minimum at the design condition for the SMC016 nozzle and is consistent with the experimental results of Tam and Tanna.[6] The OASPL of the FSMN from all three nozzles are very similar and are within 1 dB of each other.

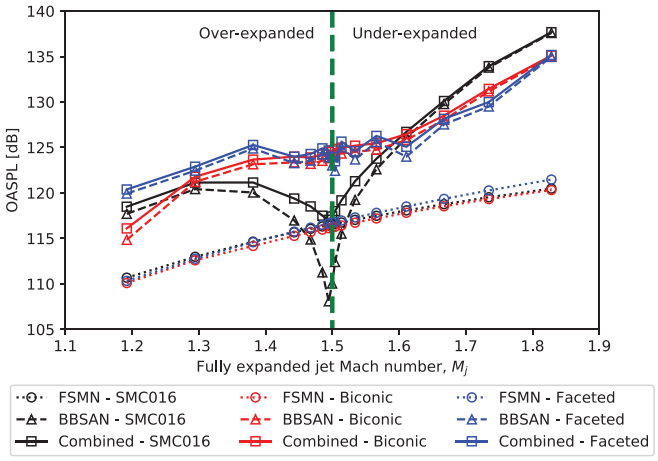

FIG. 4. (Color online) Comparison of OASPL for SMC016, bi-conic, and faceted nozzles at different NPR.

C. Effect of jet operating conditions

The sensitivity analyses of FSMN and BBSAN are performed using the SMC016 nozzle and an axisymmetric bi-conic nozzle. For the sensitivity analyses, NPR values of 2.400, 2.750, 3.100, 3.382, 3.503, 3.593, 3.643, 3.670, 3.693, 3.745, 3.858, 4.043, 4.320, 4.700, 5.200, and 6.000 are chosen. The SMC016 nozzle is operated at TTR = 1.0 and the bi-conic nozzle is operated at TTR = 3.0. The observer is located in the sideline direction at a distance of *100D*. Note that we are using unheated jet operating conditions for the SMC016 nozzle when compared to the heated jet with TTR = 3.0 used in Sec. III B.

1. Nozzle Pressure Ratio

The sensitivity analyses of FSMN and BBSAN for the SMC016 nozzle and the bi-conic nozzle are shown in Figs. 5 and 6, respectively, when the NPR is perturbed by 1% of the design NPR. The OASPL and change in OASPL are plotted against the fully-expanded jet Mach number for both the nozzles. The OASPL of FSMN and BBSAN components, and their sensitivity are plotted in Figs. 5(a) and 6(a) for SMC016 and bi-conic nozzles, respectively. The shaded regions in Figs. 5(a) and 6(a) denote the difference

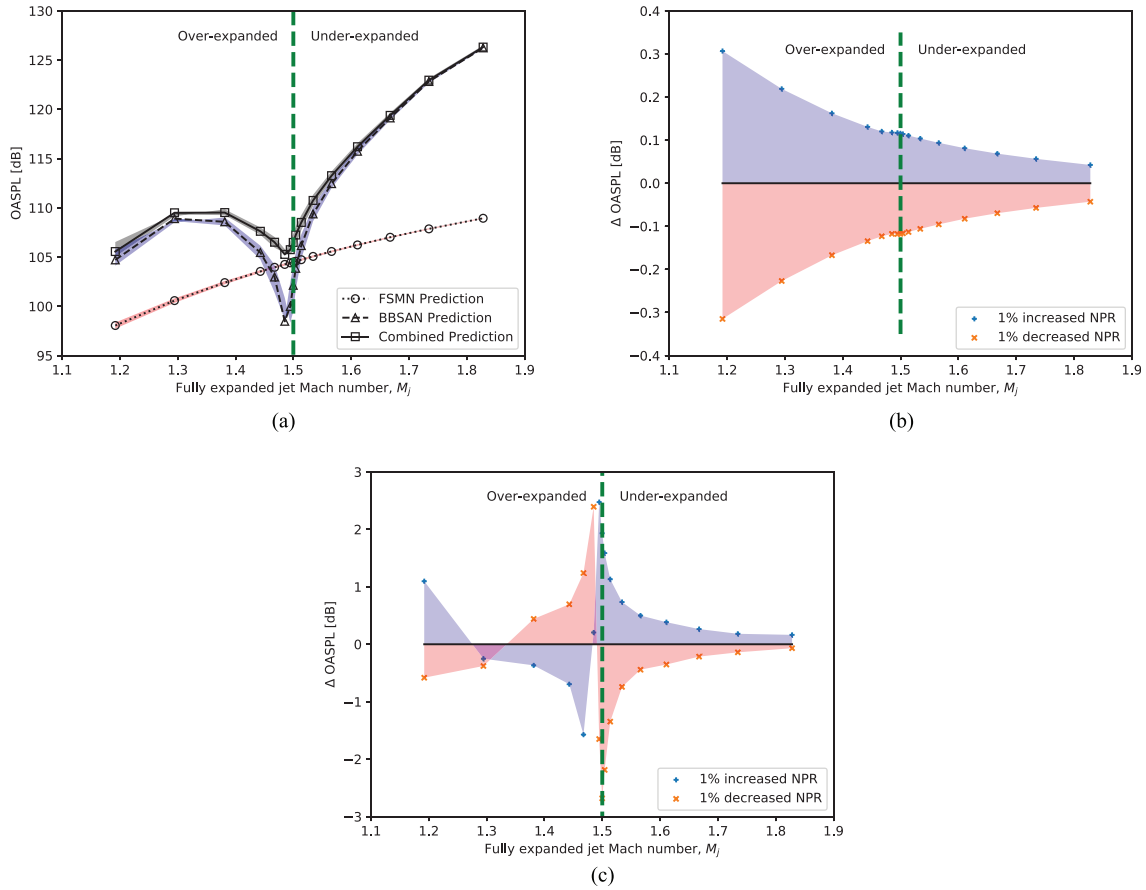

FIG. 5. (Color online) Sensitivity studies for an SMC016 nozzle with perturbed NPR. The shaded regions represent the sensitivity of noise with 1% NPR perturbations. (a) OASPL of the FSMN, BBSAN, and combined FSMN and BBSAN. (b) Δ dB change of FSMN OASPL from the base cases. (c) Δ dB change of BBSAN OASPL from the base cases.

between the perturbed case and the base case. The change in OASPL of FSMN because of small perturbations in the NPR for SMC016 nozzle and bi-conic nozzle is plotted in Figs. 5(b) and 6(b), respectively. Similarly, the change in OASPL of BBSAN for SMC016 nozzle and bi-conic nozzle is plotted in Figs. 5(c) and 6(c), respectively.

As FSMN and BBSAN are the most dominant components in the sideline direction when the jet is operating at slightly imperfectly expanded conditions, the sensitivity with perturbed input parameters is most apparent in this direction. The maximum change in the OASPL with perturbation in NPR is 0.3 and 2.8 dB for FSMN and BBSAN, respectively. For the FSMN, Figs. 5(b) and 6(b) shows that increasing the NPR by 1% increases the radiated FSMN noise and decreasing the NPR by 1% decreases the radiated noise for both nozzles. However, for the BBSAN, Fig. 5(c) shows that increasing the NPR by 1% from the base case decreases the OASPL of BBSAN at over-expanded conditions. At under-expanded conditions, increasing the NPR by 1% increases the BBSAN OASPL. This is because it moves closer to the design condition in the former case, while it moves away from the design condition in the latter case. The sensitivity of the NPR for the bi-conic nozzle is lower in comparison to the SMC016 nozzle. The maximum sensitivity with perturbed NPR is 0.25 dB at NPR = 2.40 for FSMN and 1 dB at the NPR = 2.75 for BBSAN, as observed in Figs. 6(b) and 6(c), respectively.

2. Total Temperature Ratio

For both nozzles, perturbing the TTR does not have any major effect on FSMN or BBSAN. BBSAN is the least sensitive to the TTR[23] among all the input parameters. We also observe very small variation in the sensitivity of FSMN and BBSAN at different operating conditions when the TTR is perturbed for both nozzles. Hence, for conciseness, the sensitivity plots when the TTR is perturbed by 1% are not shown in the present work. The sensitivity of TTR perturbations for the SMC016 nozzle are 0.13 and 0.15 dB for FSMN and BBSAN, respectively at all operating conditions. We also observe slight fluctuations in the change in OASPL near design condition for the SMC016 nozzle as no shock-cells are present at the design condition. The sensitivity with perturbed TTR is less than 0.2 dB for all jet operating conditions for the bi-conic nozzle. The FSMN OASPL also varies by 0.13 dB for the bi-conic nozzle at all operating conditions. This is consistent with the experimental observations of Tanna.[15]

https://doi.org/10.1121/10.0005626

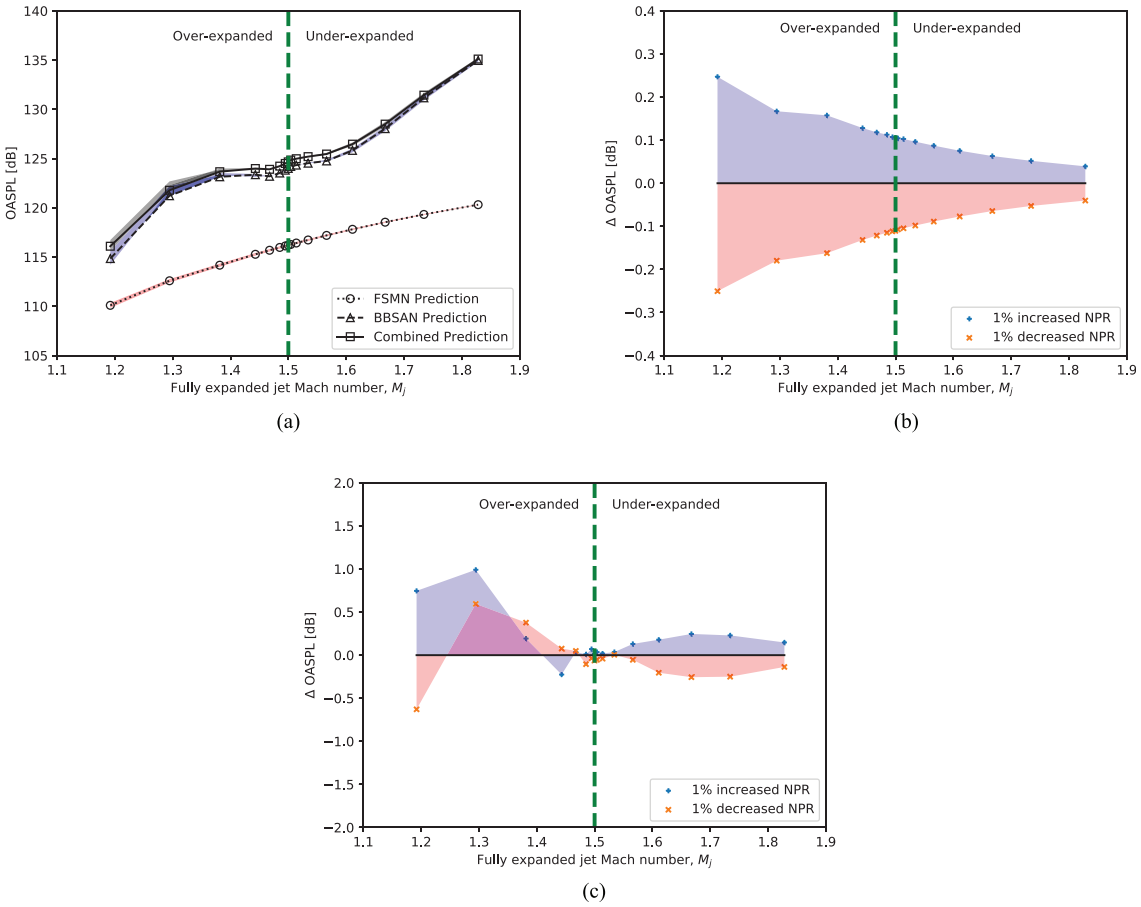

FIG. 6. (Color online) Sensitivity studies for a bi-conic nozzle with perturbed NPR. The shaded regions represent the sensitivity of noise with 1% NPR perturbations. (a) OASPL of the FSMN, BBSAN, and combined FSMN and BBSAN. (b) Δ dB change of FSMN OASPL from the base cases. (c) Δ dB change of BBSAN OASPL from the base cases.

3. Area ratio

We design new nozzle contours in order to perturb the area ratio by 1%. Perturbation of the area ratio for the bi-conic nozzle is performed by joining a straight line from the nozzle throat to the perturbed nozzle exit. For the SMC016 nozzle case, we use a MOC tool developed by Rice[56] to design a MOC nozzle with 1% increased or decreased area ratio.

The OASPL plots for FSMN and BBSAN for two different nozzles are shown in Figs. 7 and 8, respectively. The maximum sensitivity of FSMN and BBSAN OASPL with area ratio for the SMC016 nozzle is 0.17 and 5.8 dB, respectively. BBSAN is the most sensitive to the area ratio,[23] as observed from Figs. 7 and 8. Increasing and decreasing the area ratio by 1% changes the design Mach number of the nozzle to 1.517 and 1.482, respectively. This is observed in Fig. 7(a), where the minimum intensity shifts either to the left or right side of the base case, depending on whether the area ratio is increased or decreased. However, since the fully expanded jet Mach number is constant, not much effect is observed in the FSMN as shown in Fig. 7(b). Figure 7(c) shows that the OASPL decreases for over-expanded conditions by 3 dB and increases by 5.0 dB for under-expanded conditions when the area ratio is decreased. If the area ratio is increased, the SPL increases by 5.8 dB for over-expanded conditions and reduces by 2.2 dB for under-expanded conditions.

The maximum BBSAN sensitivity with perturbed area ratio is observed to be 1 dB at NPR = 4.32 for the bi-conic nozzle case shown in Fig. 8(c). Correspondingly, less than 0.1 dB change is observed in the FSMN sensitivity for the bi-conic nozzle with perturbed area ratio. A shock-cell structure is always present for the bi-conic nozzle. Hence, the reduction of noise does not occur as rapidly at the design condition as the MOC designed nozzle. Hence, for all the perturbed parameters, the unheated SMC016 nozzle is found to be more sensitive compared to the heated bi-conic nozzle.

D. Effect of boundary layer thickness at nozzle exit

We now investigate the effect of boundary layer thickness on the radiated FSMN and BBSAN. The changes in the boundary layer statistics affect the growth and decay of the instability wave in the shear layer of the jet, which directly affects FSMN and BBSAN. Furthermore, the effective area at the exit of the nozzle reduces with increase in boundary layer thickness, which modifies the shock-cell structure in the jet exhaust. We use three different methods, i.e., extension of the convergent section, a forward step at the inlet,

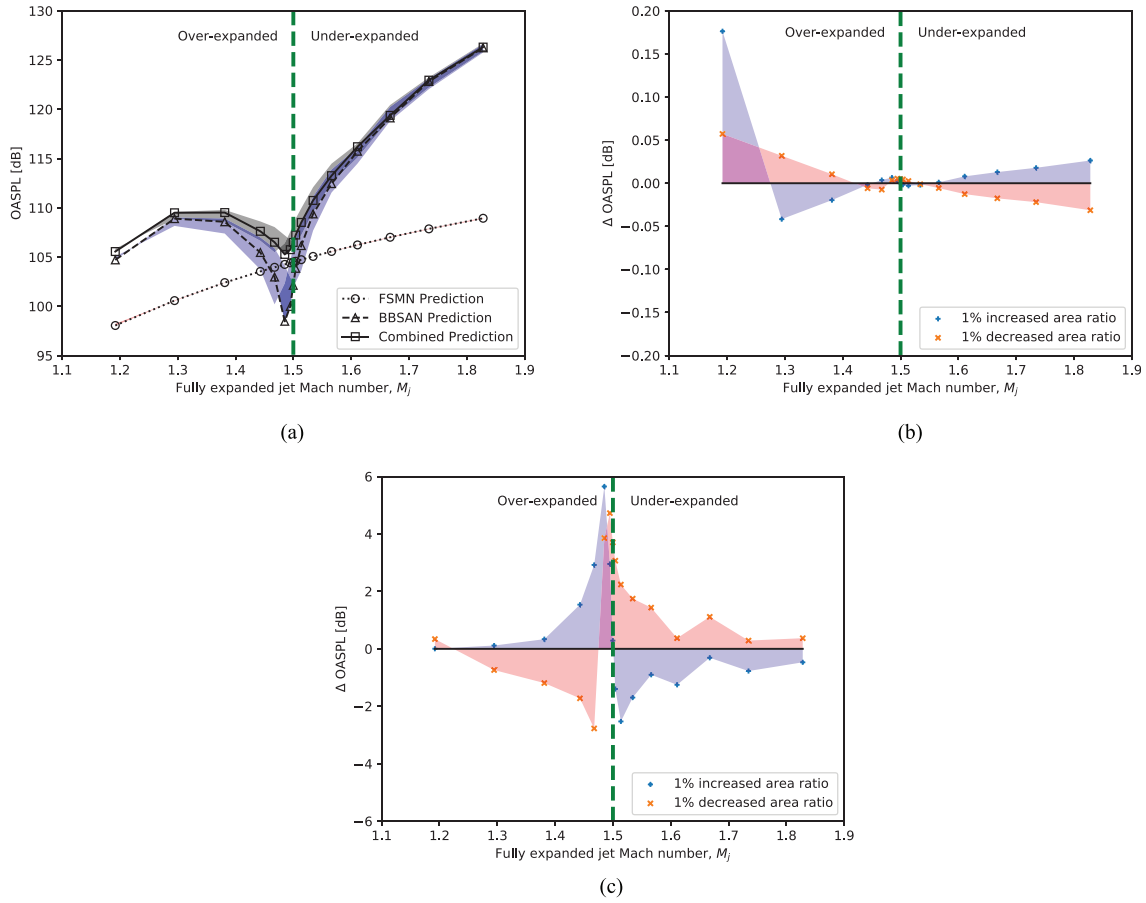

FIG. 7. (Color online) Sensitivity studies for an SMC016 nozzle with perturbed area ratio. The shaded regions represent the sensitivity of noise with 1% area ratio perturbations. (a) OASPL of the FSMN, BBSAN, and combined FSMN and BBSAN. (b) Δ dB change of FSMN OASPL from the base cases. (c) Δ dB change of BBSAN OASPL from the base cases.

and a backward step at the inlet to alter the boundary layer thickness at the nozzle exit. The forward and backward steps offer less control of the boundary layer thickness at the nozzle exit. The thickness of the boundary layer can be precisely controlled by varying the length of the converging section of the nozzle.[30] However, extending the length of the nozzle increases the number of grid points in the domain and the computational expense increases.

All three cases, i.e., the extension of nozzle inlet, forward step, and backward step are simulated using the SMC016 nozzle operating at NPR = 5.2 and TTR = 1.0. The convergent section is extended by 9D for the extended length case and a step height of 0.03D is used for the forward and backward steps. The extension length and the step height are chosen such that the computational expense is not drastically increased. The boundary layer profiles in terms of non-dimensionalized velocity and turbulent kinetic energy are plotted in Figs. 9(a) and 9(b) using inner and outer coordinates, respectively. The boundary layer is thickest for the backward facing step as observed from Fig. 9(b). Using Eqs. (3) and (4), a maximum reduction of 2.7% of the spectral density of pressure is observed when the backward facing step is used to modify the boundary layer thickness. Correspondingly, the spectral density reduces by 1.5% and 1.6% for the nozzle extension and forward facing step, respectively, when compared to the baseline SMC016 nozzle. Hence, we use the backward facing step for evaluating the change in OASPL in the sideline direction at different operating conditions due to the changes in the boundary layer thickness.

We simulate the supersonic jet cases at different operating conditions using the backward facing step for the SMC016 and biconic nozzles. The effect of the variation in the statistics of the boundary layer on the OASPL in the sideline direction is shown in Figs. 10 and 11 for the SMC016 and the bi-conic nozzles, respectively. A maximum reduction of 1.5 dB for BBSAN is observed at NPR = 3.67 for the SMC016 nozzle. We observe that the OASPL increases with increasing boundary layer thickness for the over-expanded cases. The OASPL of the FSMN is reduced by 0.08 dB at all operating conditions. The maximum reduction in the bi-conic nozzle is 0.15 dB for BBSAN. The FSMN reduces by 0.05 dB for all jet operating conditions for the bi-conic nozzle. A reduction of 5 to 6 dB is observed for the bi-conic nozzle at NPR = 2.40. This is due to flow separation occurring inside the nozzle at this operating condition. Similar to the SMC016 nozzle case, a slight increase in 0.1 dB at over-expanded conditions is observed for the bi-conic nozzle. The low reduction in noise (< 0.2 dB) at other conditions is due to the abrupt change between the

https://doi.org/10.1121/10.0005626

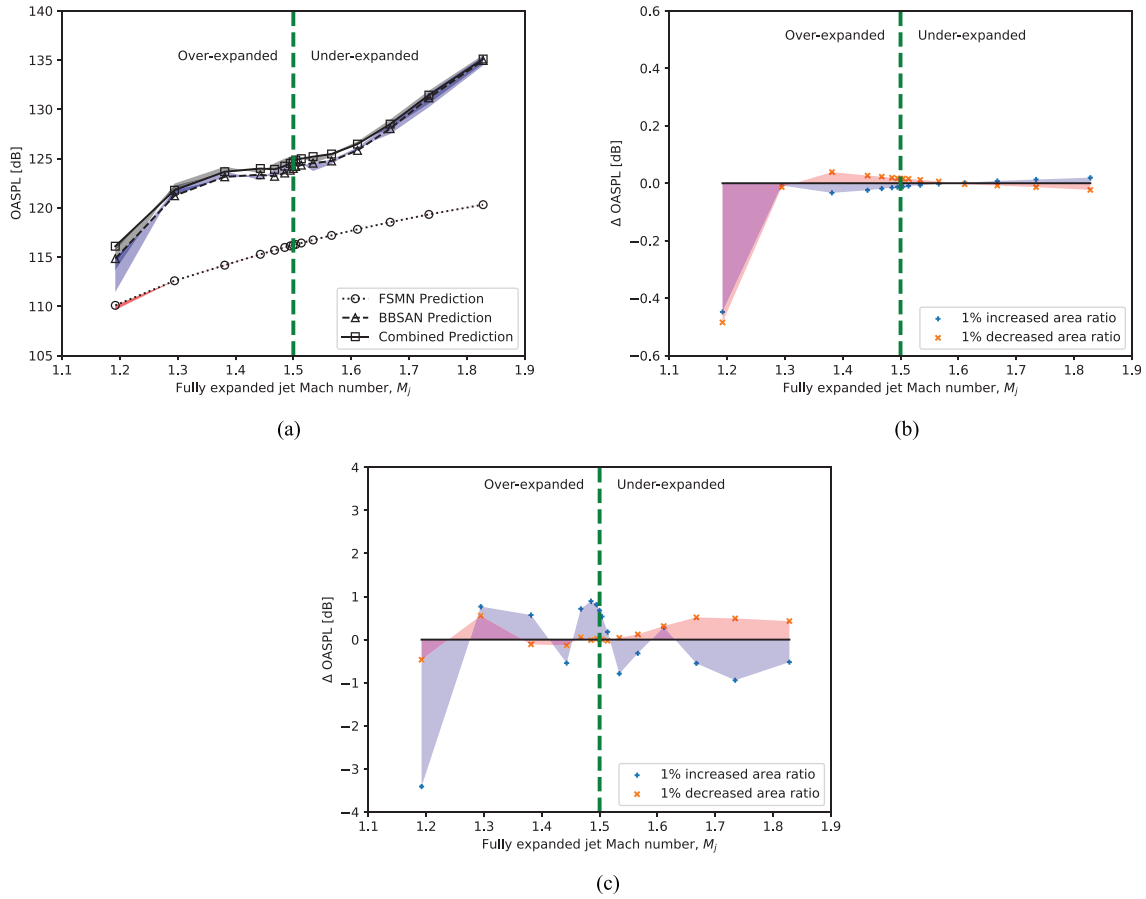

FIG. 8. (Color online) Sensitivity studies for a bi-conic nozzle with perturbed area ratio. The shaded regions represent the sensitivity of noise with 1% area ratio perturbations. (a) OASPL of the FSMN, BBSAN, and combined FSMN and BBSAN. (b) Δ dB change of FSMN OASPL from the base cases. (c) Δ dB change of BBSAN OASPL from the base cases.

converging and diverging section. The abrupt change between the converging and diverging sections induces turbulence in the boundary layer. Hence, the boundary layer thickness at the exit of the nozzle is not affected much by the backward facing step near the nozzle inlet. So, very little reduction of the FSMN and BBSAN is observed for the bi-conic nozzle.

IV. EFFECT OF FLUIDIC INJECTION

A fluidic insert is an active noise reduction technique for supersonic jets and can be turned off when required. The fluidic inserts can be turned on near airports or aircraft carriers and turned off after takeoff or away from the communities. Fluidic injection reduces supersonic jet noise by reducing the effective area at the exit of the nozzle by introducing stream-wise vortices, and by breaking down shock-cells into smaller structures. The fluidic inserts[41] were designed to mimic the aerodynamic and acoustic characteristics of nozzle corrugations.[39] However, unlike the static corrugations, fluidic inserts have the added benefit of altering the flow with changing engine set point.

In the current work, we follow the design method of Morris *et al.*[41] with minor modifications. A schematic diagram of the nozzle cross section through the fluidic injectors is shown in Fig. 12. A total of eight fluidic injection ports are placed within the previously examined faceted nozzle. We place the fluidic injectors on four facets, each separated by a 90° azimuthal angle. Symmetric positioning of fluidic injectors is used to save computational expense *via* use of symmetric boundary conditions with FUN3D. The injector ports are located at a distance of 20% and 70% of the divergent section relative to the nozzle throat. Angles of the fluid injection ports are 45°and 90°, respectively, relative to the jet upstream direction. The diameter of the injector is 2.54 mm, which corresponds to $D_{inj} = 0.05D$ to minimize the injected fluid mass flow rate. The design Mach number of the fluidic insert nozzle in the present study is unchanged relative to the faceted nozzle. This facilitates comparisons between the baseline faceted nozzle and the fluidic injection nozzle.

An additional boundary condition at the fluidic injectors is specified *via* the injector pressure and temperature ratios. The injector pressure ratio (IPR) is defined as the ratio of the stagnation pressure at the inlet of the injectors to the ambient pressure. Similarly, the injector temperature ratio (ITR) is defined as the ratio of the stagnation temperature at the inlet of injectors to the ambient temperature. The fluidic insert nozzle is operated at NPR = [2.750, 3.100, 3.670, 4.320, 5.200] and TTR = 3.0. Most of the past research on

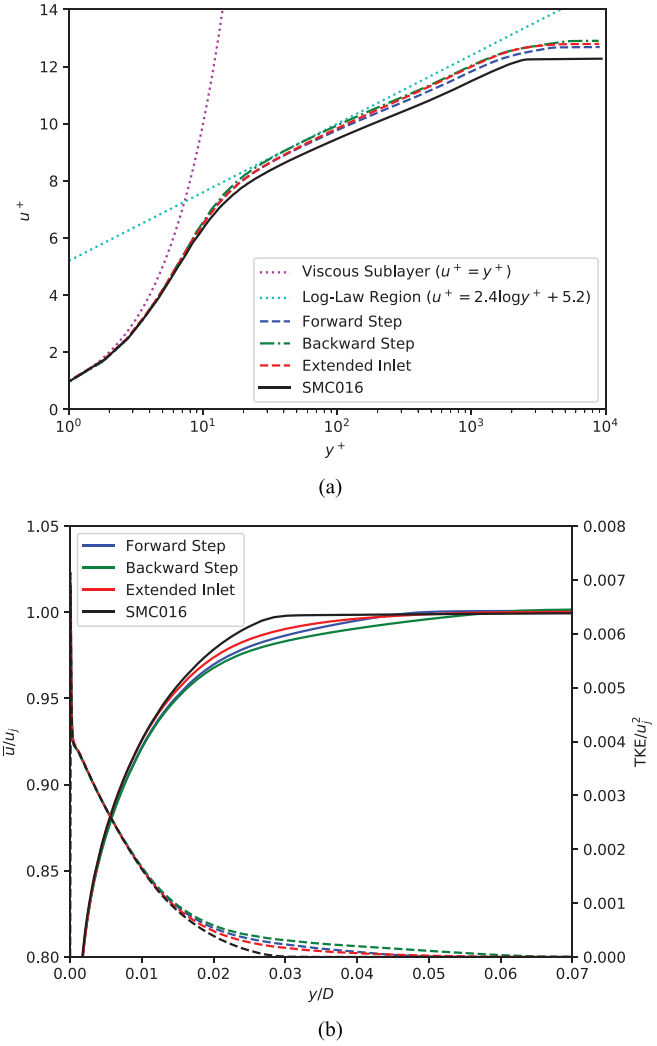

FIG. 9. (Color online) Boundary layer profiles. (a) Boundary layer profile in inner coordinates. (b) Boundary layer profile in outer coordinates. The solid lines represent the mean axial velocity, and the dashed lines represent the turbulent kinetic energy.

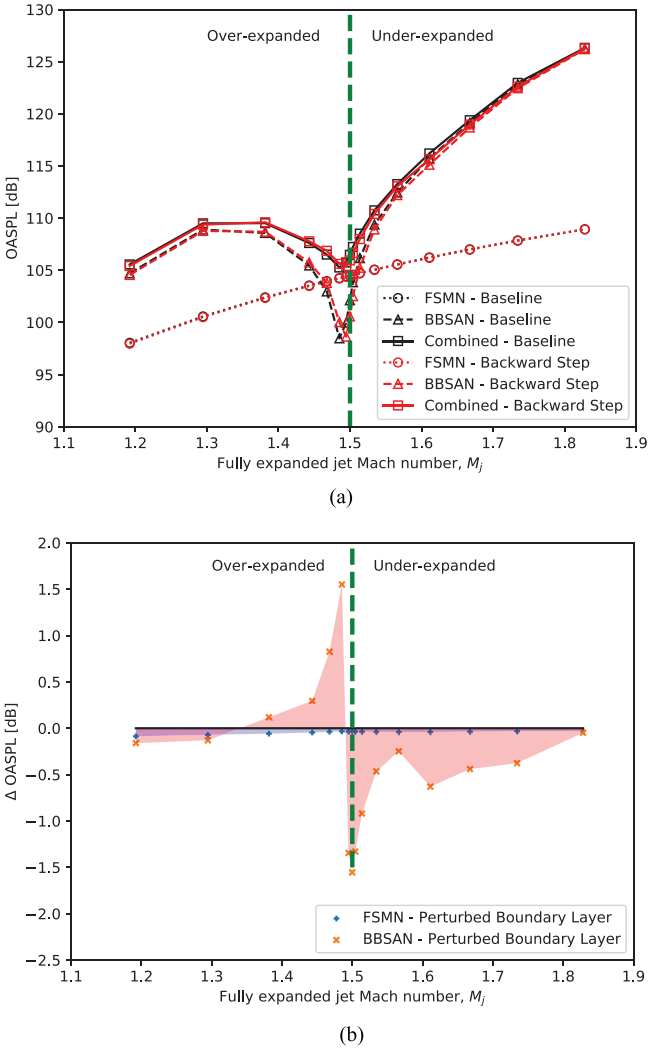

FIG. 10. (Color online) Effect of boundary layer on the FSMN and BBSAN using SMC016 nozzle. (a) OASPL of FSMN and BBSAN. (b) Δ dB change of FSMN and BBSAN OASPL.

fluidic injection[41,45,46,48–50] investigated noise reduction at over-expanded operating conditions. However, five different operating conditions, two over-expanded conditions (NPR = 2.750 and 3.100), one on-design condition (NPR = 3.670), and two under-expanded conditions (NPR = 4.320 and 5.200) are simulated in the current work. Different injector pressure ratios have been studied for the fluidic injection cases.[41,45,46,48–50] In the present study, we elect to equate IPR to NPR and an unheated ITR for the fluidic injection jet is used.

A. Aerodynamic flow-field results

The aerodynamic flow-field results of the fluidic insert nozzle are compared with the faceted nozzle for NPR = 2.750 in Figs. 13 and 14. A comparison of the numerical schlieren between the fluidic insert nozzle and the faceted nozzle is performed in Fig. 13. The numerical schlieren is plotted at a 45° azimuth cross section plane through the fluidic injectors to visualize the effect of fluidic injection. Because of the fluidic injection, the effective area at the nozzle exit is reduced and an altered shock-cell structure near the nozzle exit is observed. The length-scale and time-scale are increased by 20% and 45%, respectively, along the lip-line in the plane of the fluidic inserts due to the thicker boundary layer when compared to the faceted nozzle. Because of the complicated interaction of different shock-cell structures, the shock-cells break down into smaller structures. Hence, the length of the potential core is also reduced for all fluidic insert nozzle cases. The length of the potential core of the fluidic insert nozzle reduces by approximately 40% to 45% of the faceted nozzle potential core length for all operating conditions.

The cross-stream contours of Mach number and turbulent kinetic energy at different axial locations for the fluidic insert nozzle operating at an NPR = 2.750 is plotted in Fig. 14. The alteration of the flow-field due to the fluidic injectors can be observed at the cross-sectional planes near the nozzle exit. Complicated cross-sectional contours of Mach number and TKE are observed until $x/D = 3$. The

https://doi.org/10.1121/10.0005626

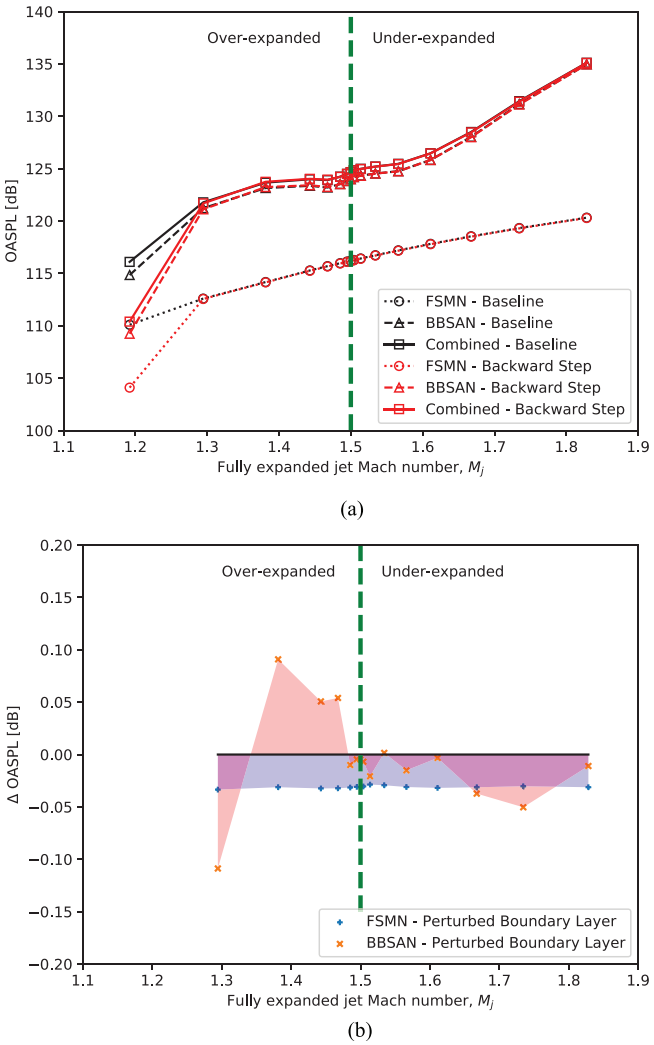

FIG. 11. (Color online) Effect of boundary layer on the FSMN and BBSAN using biconic nozzle. (a) OASPL of FSMN and BBSAN. (b) Δ dB change of FSMN and BBSAN OASPL.

Mach number and TKE form a diamond- or square-shaped profile at the cross-sectional planes near the nozzle exit. However, at $x/D = 7.5$, similar axisymmetric contours of Mach number and TKE relative to the round nozzle are observed for all jet operating conditions. The alteration of the flow-field from the injectors is not apparent at this location and further downstream.

B. Acoustic prediction results

The OASPL predictions of the FSMN and BBSAN for the fluidic insert nozzle are performed using Eqs. (3) and (4), respectively. OASPL predictions in the sideline direction from the fluidic insert nozzle cases and the faceted nozzle cases are plotted in Fig. 15. The fluidic injection reduces the FSMN OASPL by 1.75 dB for all jet operating conditions. The fluidic injection reduces the BBSAN OASPL by 5.5 and 2 dB at the over-expanded conditions at NPR = 2.750 and NPR = 3.100, respectively. A similar 2 to 6 dB noise reduction has been observed for different over-expanded jet operating conditions by Morris *et al.*[41] However, the BBSAN OASPL increases for the on-design and under-expanded jet operating conditions because an effect of the fluidic injection is to further decrease the expansion of the flow within the nozzle, pushing the jet further from its design conditions. The maximum increase in BBSAN OASPL is 5 dB which, is observed at NPR = 4.320. Since fluidic injection is an active noise reduction mechanism, it can be turned off for under-expanded jet operating conditions.

Fluidic injection introduces stream-wise vorticity that reduces the TKE for the fine-scale turbulence in the shear layer.[48] The shock-cell structure and the effective exit area of the jet are also modified due to the fluidic injection.[48] For over-expanded conditions, reducing the effective exit area of the jet shifts the operating condition of the jet closer to the on-design condition; thereby reducing BBSAN. The changes in the OASPL can also be attributed to the breakdown of the shock-cell structure due to the fluidic injection. However, for an under-expanded jet operating condition, reducing the effective exit area of the jet increases the off-design jet parameter, β. This causes an increase in noise for the under-expanded jet conditions.

C. Source locations

We ascertain the source term intensity directly from the RANS CFD solutions. The contours of the identified source term for FSMN and BBSAN are plotted in Figs. 16(a) and 16(b), respectively, for NPR = 2.750 and TTR = 3.0. The contours of FSMN and BBSAN sources are plotted using Eqs. (1) and (2), respectively. For all the jet operating

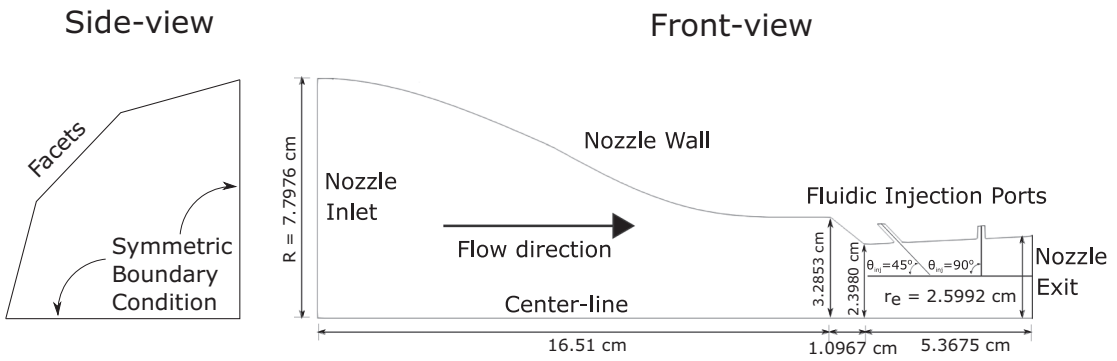

FIG. 12. Schematic diagram of two fluidic injectors in the diverging section of the faceted nozzle.

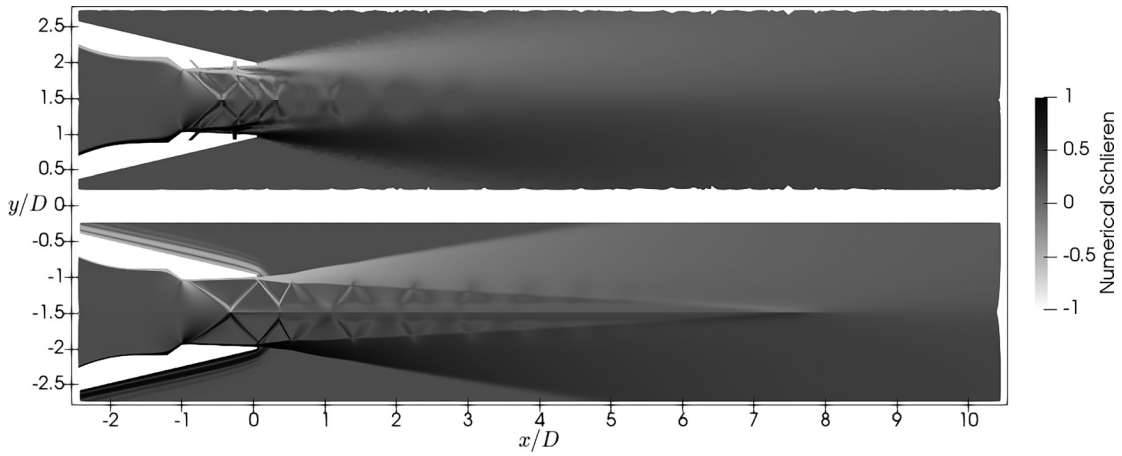

FIG. 13. Comparison of the numerical schlieren between (top) the fluidic insert nozzle case and (bottom) the baseline faceted nozzle case operating at NPR=2.750 and TTR=3.0.

conditions, we observe that the FSMN and BBSAN sources shift closer to the nozzle exit for the fluidic insert nozzle when compared to the faceted nozzle. The length of the potential core also decreases by 40% to 45% for all operating conditions for the fluidic insert nozzle cases, resulting in the shift of the FSMN and BBSAN sources close to the nozzle exit.

Fluidic injection reduces the total FSMN source term intensity in the shear layer of the jet for all operating conditions. The FSMN source term intensity is reduced by 40% at

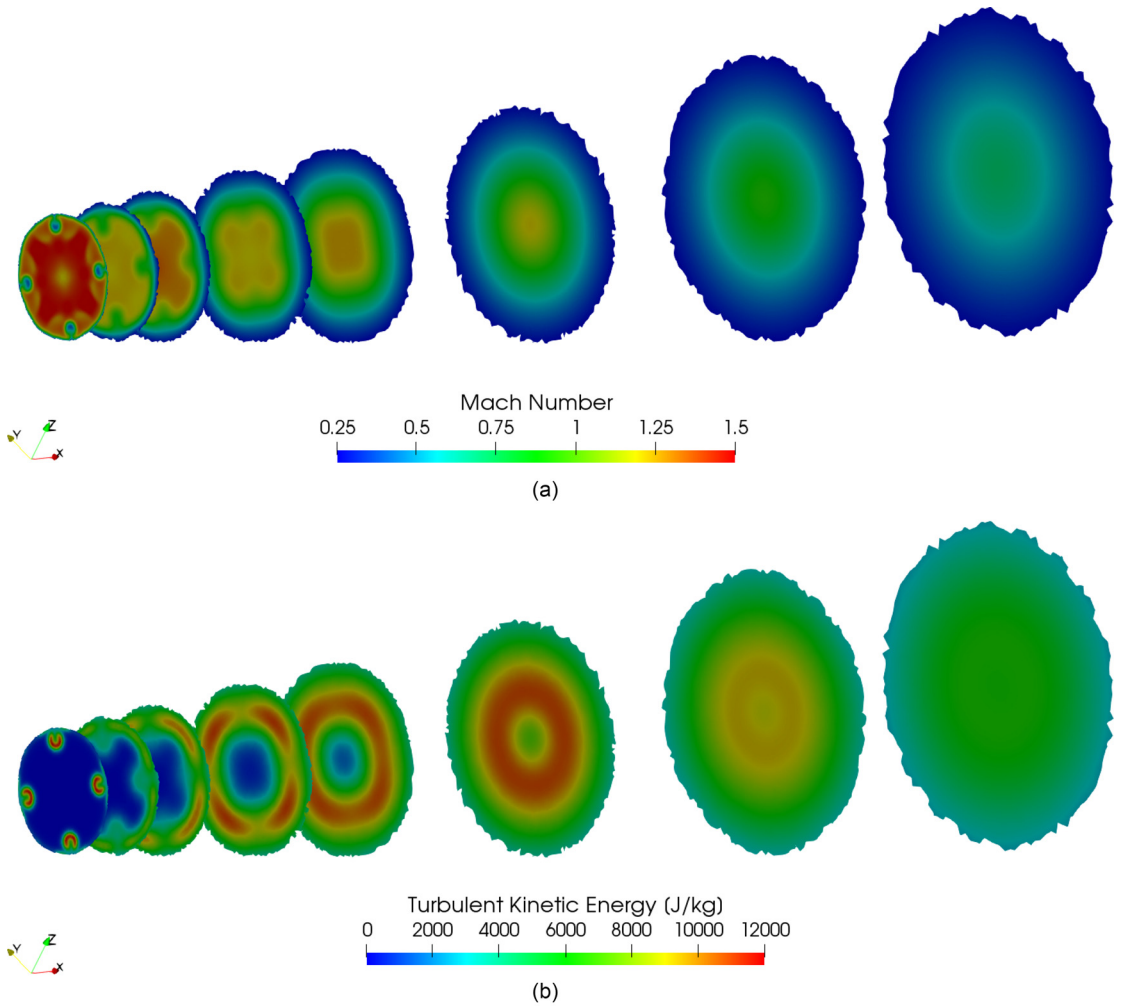

FIG. 14. (Color online) Cross-stream contours of at different axial locations, $x/D = 0$, 0.5, 1.0, 2.0, 3.0, 5.0, 7.5, and 10.0 for the fluidic insert nozzle operating at NPR = 2.750 and TTR = 3.0. (a) Contours of Mach number. (b) Contours of turbulent kinetic energy.

https://doi.org/10.1121/10.0005626

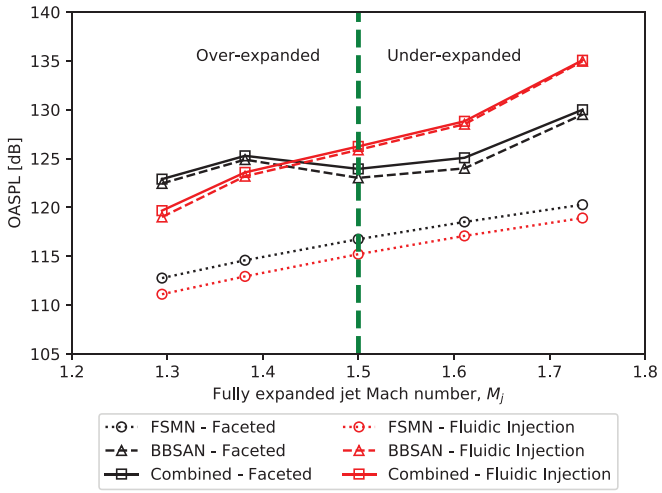

FIG. 15. (Color online) Comparison of the OASPL between the fluidic insert nozzle cases and the faceted nozzle cases at different operating conditions in the sideline direction.

the downstream locations. However, an increase of 2.92% of the maximum FSMN source term intensity is observed in the plane of fluidic inserts. The maximum FSMN sources are located between 11D to 19D for the NPR = 2.750 and 5.200, respectively, for the faceted nozzle. For the fluidic injection nozzle, the sources shift upstream and are located between 8D to 13D for NPR = 2.750 and 5.200, respectively.

Compared to the FSMN reduction at all jet operating conditions, the BBSAN source term intensity is reduced only for the over-expanded cases. A maximum reduction of the source term intensity of 35% is observed at the intersection between the shock-cells and shear layer region for the NPR = 2.750 operating condition. However, the BBSAN source term intensity increases by 193% for the NPR = 5.200 operating condition. This is due to the reduction of effective area at the nozzle exit that occurs from fluidic injection that increases the off-design parameter for under-expanded cases. The BBSAN source term intensity is high near the nozzle exit due to the complicated shock-cell structure present near the nozzle exit.

Note that the comparisons of the fluidic injection nozzle to the faceted nozzle were performed on NPR or fully-expanded jet Mach number basis. However, the decrease in the effective area due to the fluidic injection may result in a decrease in the specific thrust of the nozzle. To calculate the specific thrust, we make similar assumptions as Prasad and Morris.[57] The bypass ratio is assumed to be 0.3 and the bypass exit velocity is assumed to be 60% of the fully-expanded jet velocity. Thrust reduction of approximately 4% at NPR = 2.750 to 6% at NPR = 5.20 was observed. Hence, additional analyses on the reduction of noise by

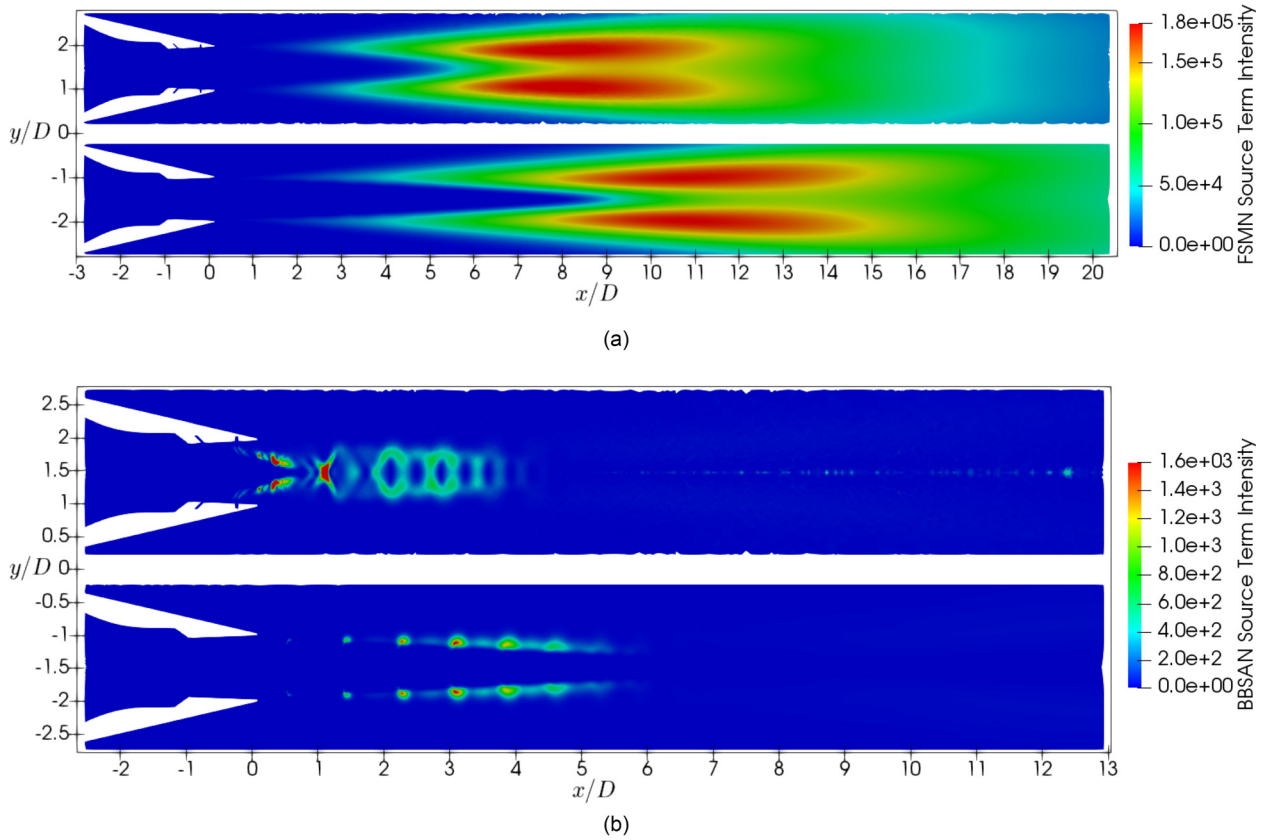

FIG. 16. (Color online) Comparison of the contours of FSMN and BBSAN source locations between (top) the fluidic injection nozzle and (bottom) the faceted nozzle operating at NPR = 2.750 and TTR = 3.0. (a) FSMN source locations. (b) BBSAN source locations.

matching specific thrust levels are necessary in the future to accurately quantify the noise reduction.

V. SUMMARY AND CONCLUSIONS

Various analyses of the FSMN and BBSAN using the developed statistical models have been performed for the purpose of ascertaining the sensitivity with different parameters. We observed that the sensitivity of all parameters was less than 0.13 and 1 dB for FSMN and BBSAN models, respectively. The convective velocity was found to be the most sensitive parameter for the BBSAN model while the length-scale and timescale were the most sensitive parameters for the FSMN model. A comparison of the noise radiated from different nozzle geometries, a MOC nozzle, a bi-conic nozzle, and a faceted nozzle has been performed. We observed that the noise radiated in terms of OASPL from the bi-conic nozzle and faceted nozzle was within 2 dB of each other in the sideline direction.

We also analysed the effect of perturbing the NPR, TTR, area ratio, and exit boundary layer profile. We observed that the BBSAN was most sensitive to area ratio and least sensitive to the TTR. The FSMN was least sensitive to area ratio and most sensitive to NPR. For BBSAN, the MOC nozzle was found to be more sensitive than the bi-conic nozzle due to the elimination of shock-cells when operating at the design condition. The sensitivity of FSMN was observed to be similar for both nozzle types. A maximum reduction of 1.5 dB near the design condition for the SMC016 nozzle was observed with a small perturbation of the exit boundary layer profile.

Finally, we analysed the fluidic injection noise reduction technique using the developed statistical models. The design of the fluidic insert ports closely followed the work of Morris *et al.*[41] A reduction of 6 dB was observed for the over-expanded case at NPR = 2.75, while an increase in 4–5 dB was observed for under-expanded cases. The source locations for BBSAN and FSMN are also plotted using the identified source terms. The source locations shift upstream towards the nozzle exit for the fluidic injection case compared with the baseline faceted nozzle. The reduction at over-expanded cases was observed to be consistent with experimental measurements.[41]

ACKNOWLEDGMENTS

This research was supported by the Office of Naval Research Grant No. N00014-17-1-2583. Any opinions, findings, and conclusions or recommendations expressed in this material are those of the author(s) and do not necessarily reflect the views of the Office of Naval Research.

[1]J. Doychak, "Department of Navy Jet Noise Reduction Project Overview," in *Proceedings of the 15th Annual Partners in Environmental Technology Technical Symposium and Workshop*, Washington, DC (November 30 – December 2, 2010).
[2]T. K. Patel and S. A. E. Miller, "Statistical sources for broadband shock-associated noise using the Navier-Stokes equations," J. Acoust. Soc. Am. **146**(6), 4339–4351 (2019).
[3]T. K. Patel and S. A. E. Miller, "Source of fine-scale turbulent mixing noise using the Navier–Stokes equations," AIAA J. **59**(6), 2333–2338 (2021).
[4]C. K. W. Tam, "Supersonic jet noise," Ann. Rev. Fluid Mech. **27**(1), 17–43 (1995).
[5]M. Harper-Bourne and M. J. Fisher, "The noise from shocks waves in supersonic jets," NATO AGARD-CP-131 11 (NATO, Brussels, Belgium, 1973).
[6]C. K. W. Tam and H. K. Tanna, "Shock associated noise of supersonic jets from convergent-divergent nozzles," J. Sound Vib. **81**(3), 337–358 (1982).
[7]C. K. W. Tam, "Stochastic model theory of broadband shock associated noise from supersonic jets," J. Sound Vib. **116**(2), 265–302 (1987).
[8]P. J. Morris and S. A. E. Miller, "Prediction of broadband shock-associated noise using Reynolds-averaged Navier-Stokes computational fluid dynamics," AIAA J. **48**(12), 2931–2944 (2010).
[9]T. Suzuki, "Wave-packet representation of shock-cell noise for a single round jet," AIAA J. **54**(12), 3903–3917 (2016).
[10]C. K. W. Tam and L. Auriault, "Jet mixing noise from fine-scale turbulence," AIAA J. **37**(2), 145–153 (1999).
[11]S. A. E. Miller, "Noise from Isotropic Turbulence," AIAA J. **55**(3), 755–773 (2017).
[12]M. Dahl and A. Khavaran, "The effect of nondeterministic parameters on shock-associated noise prediction modeling," in *Proceedings of the 16th AIAA/CEAS Aeroacoustics Conference*, Stockholm, Sweden (June 7–9, 2010), AIAA Paper No. 2010-3841.
[13]J. B. Freund, "Adjoint-based optimization for understanding and suppressing jet noise," J. Sound Vib. **330**(17), 4114–4122 (2011).
[14]J. Kim, D. J. Bodony, and J. B. Freund, "Adjoint-based control of loud events in a turbulent jet," J. Fluid Mech. **741**, 28–59 (2014).
[15]H. K. Tanna, "An experimental study of jet noise. Part II: Shock associated noise," J. Sound Vib. **50**(3), 429–444 (1977).
[16]J. M. Seiner and T. D. Norum, "Experiments of shock associated noise of supersonic jets," in *Proceedings of the 12th Fluid and Plasma Dynamics Conference*, Williamsburg, VA (July 23–25, 1979), AIAA Paper No. 79-47341.
[17]J. M. Seiner and T. D. Norum, "Aerodynamic aspects of shock containing jet plumes," in *Proceedings of the 6th Aeroacoustics Conference*, Hartford, CT (June 4–6, 1980), AIAA Paper No. 80-43600.
[18]T. D. Norum and J. M. Seiner, "Location and propagation of shock associated noise from supersonic jets," in *Proceedings of the 6th Aeroacoustics Conference*, Hartford, CT (June 4–6, 1980), AIAA Paper No. 80-43599.
[19]T. D. Norum and J. M. Seiner, "Measurements of mean static pressure and far-field acoustics of shock-containing supersonic jets," NASA/TM-84521 19820025274 (NASA, Washington, DC, 1982).
[20]T. D. Norum and J. M. Seiner, "Broadband shock noise from supersonic jets," AIAA J. **20**(1), 68–73 (1982).
[21]J. M. Seiner and J. C. Yu, "Acoustic near-field properties associated with broadband shock noise," AIAA J. **22**(9), 1207–1215 (1984).
[22]J. E. Bridges and M. P. Wernet, "Turbulence associated with broadband shock noise in hot jets," NASA/TM-2008-215274 (NASA, Washington, DC, 2008).
[23]K. Viswanathan, M. B. Alkislar, and M. J. Czech, "Characteristics of the shock noise component of jet noise," AIAA J. **48**(1), 25–46 (2010).
[24]C.-W. Kuo, D. K. McLaughlin, P. J. Morris, and K. Viswanathan, "Effects of jet temperature on broadband shock-associated noise," AIAA J. **53**(6), 1515–1530 (2015).
[25]S. A. E. Miller, "The scaling of broadband shock-associated noise with increasing temperature," Int. J. Aeroacoust. **14**(1–2), 305–326 (2015).
[26]J. Mabe, "Variable area jet nozzle for noise reduction using shape memory alloy actuators," J. Acoust. Soc. Am. **123**(5), 3871–3871 (2008).
[27]U. Michel, "The benefits of variable area fan nozzles on turbofan engines," in *Proceedings of the 49th AIAA Aerospace Sciences Meeting*, Orlando, FL (January 4–7, 2011), AIAA Paper No. 2011-226.
[28]C. K. W. Tam, M. Golebiowski, and, and J. M. Seiner, "On the two components of turbulent mixing noise from supersonic jets," in *Proceedings of the 2nd AIAA/CEAS Aeroacoustics Conference*, State College, PA (May 6–8, 1996), AIAA Paper No. 96-1716.
[29]M. Saleem, O. Lopez Rodriguez, E. Gutmark, J. Liu, and, and Y. Khine, "Noise and flow characterization of supersonic jets emanating from a circular and faceted nozzles," in *Proceedings of the AIAA Scitech 2020 Forum*, Orlando, FL (January 6–10, 2020), AIAA Paper No. 2020-1247.

[30]K. B. M. Q. Zaman, "Effect of initial boundary-layer state on subsonic jet noise," AIAA J. **50**(8), 1784–1795 (2012).
[31]C. Bogey and C. Bailly, "Influence of nozzle-exit boundary-layer conditions on the flow and acoustic fields of initially laminar jets," J. Fluid Mech. **663**, 507–538 (2010).
[32]C. Bogey, O. Marsden, and C. Bailly, "Large-eddy simulation of the flow and acoustic fields of a Reynolds number 10^5 subsonic jet with tripped exit boundary layers," Phys. Fluids **23**(3), 035104 (2011).
[33]G. A. Brès, P. Jordan, V. Jaunet, M. L. Rallic, A. V. G. Cavalieri, A. Towne, S. K. Lele, T. Colonius, and O. T. Schmidt, "Importance of the nozzle-exit boundary-layer state in subsonic turbulent jets," J. Fluid Mech. **851**, 83–124 (2018).
[34]N. P. Breen and K. K. Ahuja, "Measuring jet noise source locations with acoustic beamforming," in *Proceedings of the 53rd AIAA Aerospace Sciences Meeting*, Kissimmee, FL (January 5–9, 2015), AIAA Paper No. 2015-0735.
[35]L. Maestrello, "An experimental study on porous plug jet noise suppressor," in *Proceedings of the 5th Aeroacoustics Conference*, Seattle, WA (March 12–14, 1979), AIAA Paper No. 79-0673.
[36]J. E. Bridges, K. B. M. Q. Zaman, and B. Heberling, "Basics of mixer-ejectors for quiet propulsion," in *Proceedings of the IAA Aviation 2020 Forum*, Virtual Event (June 15–19, 2020), AIAA Paper No. 2020-2505.
[37]D. L. Huff, "Noise reduction technologies for turbofan engines," NASA/TM-2007-214495 (NASA, Washington, DC, 2007).
[38]K. Viswanathan, A. Krothapalli, J. M. Seiner, M. J. Czech, B. Greska, and B. J. Jansen, "Assessment of low-noise nozzle designs for fighter aircraft applications," J. Aircr. **48**(2), 412–423 (2011).
[39]J. M. Seiner and M. M. Gilinsky, "Nozzle thrust optimization while reducing jet noise," AIAA J. **35**(3), 420–427 (1997).
[40]N. E. Murray and B. J. Jansen, "Performance efficient jet noise reduction for supersonic nozzles," Int. J. Aeroacoust. **11**(7-8), 937–956 (2012).
[41]P. J. Morris, D. K. McLaughlin, and C.-W. Kuo, "Noise reduction in supersonic jets by nozzle fluidic inserts," J. Sound Vib. **332**(17), 3992–4003 (2013).
[42]M. Samimy, J.-H. Kim, J. Kastner, I. Adamovich, and Y. Utkin, "Active control of a Mach 0.9 jet for noise mitigation using plasma actuators," AIAA J. **45**(4), 890–901 (2007).
[43]J. A. Schetz and F. S. Billig, "Penetration of gaseous jets injected into a supersonic stream," J. Spacecr. Rockets **3**(11), 1658–1665 (1966).
[44]D. Papamoschou and D. G. Hubbard, "Visual observations of supersonic transverse jets," Exp. Fluids **14**(6), 468–476 (1993).
[45]R. W. Powers, S. Hromisin, D. K. McLaughlin, and, and P. J. Morris, "Mean velocity and turbulence measurements of supersonic jets with fluidic inserts," in *Proceedings of the 54th AIAA Aerospace Sciences Meeting*, San Diego, CA (January 4–8, 2016), AIAA Paper No. 2016-0001.
[46]D. K. McLaughlin, P. J. Morris, and S. Martens, "Scaled demonstration of fluid insert noise reduction for tactical fighter aircraft engines," J. Aircr. **56**(5), 1935–1941 (2019).
[47]C. Prasad and P. J. Morris, "Effect of fluid injection on turbulence and noise reduction of a supersonic jet," Philos. Trans. R. Soc. A **377**(2159), 20190082 (2019).
[48]P. J. Morris, D. K. McLaughlin, R. W. Powers, and, and M. J. Kapusta, "Prediction, experiments and optimization of high-speed jet noise reduction using fluidic inserts," in *Proceedings of the 50th AIAA/ASME/SAE/ASEE Joint Propulsion Conference*, Cleveland, OH (July 28–30, 2014), AIAA Paper No. 2014-3737.
[49]M. Coderoni, A. S. Lyrintzis, and G. A. Blaisdell, "Noise reduction analysis of supersonic unheated jets with fluidic injection using large eddy simulations," Int. J. Aeroacoust. **17**(4–5), 467–501 (2018).
[50]D. Cuppoletti, E. Gutmark, H. Hafsteinsson, and L.-E. Eriksson, "Elimination of shock-associated noise in supersonic jets by destructive wave interference," AIAA J. **57**(2), 720–734 (2019).
[51]R. T. Biedron, J.-R. Carlson, J. M. Derlaga, P. A. Gnoffo, D. P. Hammond, W. T. Jones, B. Kleb, E. M. Lee-Rausch, E. J. Nielsen, M. A. Park, C. L. Rumsey, J. L. Thomas, K. B. Thompson, and W. A. Wood, "FUN3D Manual 13.4," NASA/TM-2018-220096 (NASA, Washington, DC, 2018).
[52]C. Brown and J. E. Bridges, "Small hot jet acoustic rig validation," NASA/TM-2006-214234 (NASA, Washington, DC, 2006).
[53]T. K. Patel, "Analysis of supersonic jet noise in the sideline and upstream directions using the Navier-Stokes equations," Ph.D. thesis, University of Florida, Gainesville, FL, 2020.
[54]A. R. Pilon, R. W. Powers, D. K. McLaughlin, and P. J. Morris, "Design and analysis of a supersonic jet noise reduction concept," J. Aircr. **54**(5), 1705–1717 (2017).
[55]D. R. Cuppoletti, "Supersonic jet noise reduction with novel fluidic injection techniques," Ph.D. thesis, University of Cincinnati, Cincinnati, OH, 2013.
[56]T. Rice, "2D and 3D Method of characteristic tools for complex nozzle development final report," NASA/RTDC-TPS-481 (NASA, Washington, DC, 2003).
[57]C. Prasad and P. J. Morris, "Steady active control of noise radiation from highly heated supersonic jets," J. Acoust. Soc. Am. **149**(2), 1306–1317 (2021).